**Repositorio Institucional de la Universidad Autónoma de Madrid**

https://repositorio.uam.es

Esta es la **versión de autor** del artículo publicado en:
This is an **author produced version** of a paper published in:

Solid State Communications 131.9 (2004): 625-630

DOI: http://dx.doi.org/10.1016/j.ssc.2004.05.031

**Copyright:** © 2004 Elsevier Ltd

El acceso a la versión del editor puede requerir la suscripción del recurso
Access to the published version may require subscription

# Conductance properties of nanotubes coupled to superconducting leads: signatures of Andreev states dynamics

E. Vecino[1], M.R. Buitelaar[2*], A. Martín-Rodero[1], C. Schönenberger[2] and A. Levy Yeyati[1]
[1]*Departamento de Física Teórica de la Materia Condensada C-V. Universidad Autónoma de Madrid. E-28049 Madrid. Spain. and*
[2]*Institut für Physik, Universität Basel, Klingelbergstrasse 82, CH-4056 Basel, Switzerland.*
(Dated: February 2, 2008)

We present a combined experimental and theoretical analysis of the low bias conductance properties of carbon nanotubes coupled to superconducting leads. In the Kondo regime the conductance exhibits a zero bias peak which can be several times larger than the unitary limit in the normal case. This zero bias peak can be understood by analyzing the dynamics of the subgap Andreev states under an applied bias voltage. It is shown that the existence of a linear regime is linked to the presence of a finite relaxation rate within the system. The theory provides a good fitting of the experimental results.

PACS numbers: PACS numbers: 73.63.-b, 73.21.La, 74.50.+r

Carbon nanotubes connected to metallic electrodes allow to study many different regimes in mesoscopic electron transport exhibiting either ballistic or diffusive behavior [1, 2]; Luttinger liquid features [3], etc. Several experiments [4] have demonstrated that carbon nanotubes weakly coupled to normal leads can also exhibit Coulomb blockade and Kondo effect, i.e. the characteristic physics of quantum dots (QD). Very recently the research on the transport properties of this system has been extended with the inclusion of superconductivity on the leads [5]. In particular Buitelaar et al. [6] have achieved a physical realization of a S-QD-S system using carbon nanotubes coupled to Al/Au leads. Their results, showing an enhancement of the conductance in the Kondo regime with respect to the normal case, have attracted considerable theoretical attention [7, 8, 9].

From a theoretical point of view transport in a voltage biased S-QD-S system poses a challenging problem due to the interplay between electron correlation effects and multiple Andreev reflection (MAR) processes which provide the main mechanism for quasiparticle transport at small bias. This problem has been addressed by several authors at different levels of approximation. Thus, in Refs. [11] numerical results were presented for the S-QD-S system neglecting electron correlation effects. This approach has also been used by Buitelaar et al. [7] for analyzing the experimental results for the subgap structure of Ref. [6]. On the other hand, Avishai et al. [10] have introduced the effect of electron interactions at the level of the slave boson mean field approach and obtained numerical results for the current and the noise spectrum in the Kondo regime. More recently, some of us have shown that the conductance properties of a S-QD-S system in the Kondo regime can be understood in terms of the dynamics of subgap states (Andreev states) under an applied bias voltage [8].

In the present work we combine experimental and theoretical analysis in order to identify signatures of Andreev states dynamics in the low bias conductance of carbon nanotubes coupled to superconducting leads. We shall first describe the setup used for the conductance measurements and discuss the main experimental results. We then introduce the theoretical model in which we assume that the system can be appropriately analyzed as a single level quantum dot. In contrast to Ref. [8], in the present calculations we explicitly take into account the presence of a finite inelastic relaxation rate within the system. As will be shown the low bias conductance properties are extremely sensitive to this rate. The comparison with the experimental results allows to determine the size of this parameter in the actual system as well as to confirm the main predictions of the theory.

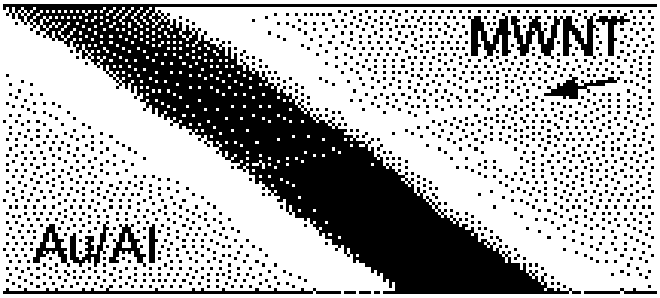


FIG. 1: Typical 2-terminal device geometry. For the measurements presented here, the electrode spacing is 0.25 $\mu$m and the MWNT length 1.5 $\mu$m. The (oxidized) Si substrate is used as a gate electrode.

The device we consider consists of an individual multiwall carbon nanotube (MWNT) of 1.5 $\mu$m length between source and drain electrodes that are separated by 250 nm, Fig.1. The lithographically defined leads were evaporated over the MWNT, 45 nm of Au followed by 135 nm of Al. The degenerately doped Si substrate was used as a gate electrode.

The device is first characterized with the contacts driven normal by applying a small magnetic field of

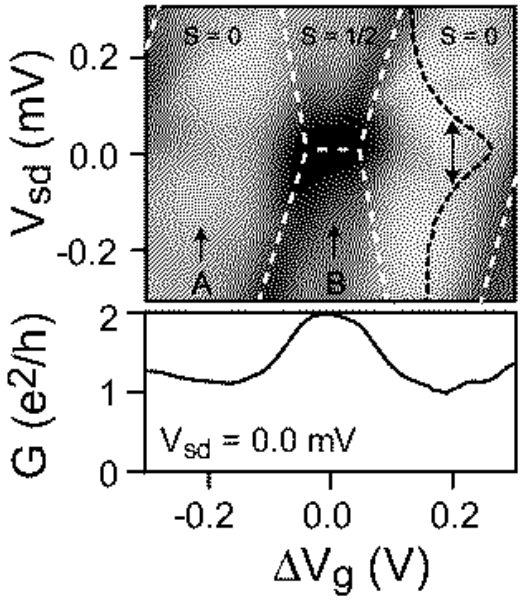


FIG. 2: Gray scale representation of the differential conductance $dI/dV$ versus source-drain ($V_{sd}$) and gate voltage ($V_g$) with the leads in the normal state (darker = more conductive). The dashed white lines outline the Coulomb blockade diamonds and the Kondo ridge. The black dashed line trace is the $dI/dV$ in the middle of the Kondo ridge (position $B$), from which $T_K$ can be estimated. The line trace in the bottom graph is the linear-response conductance.

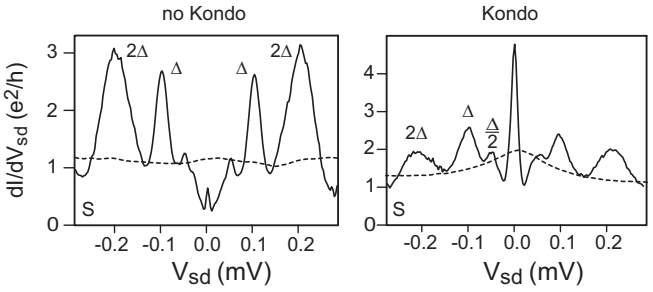


FIG. 3: Differential conductance $dI/dV$ in the middle of a Coulomb diamond (left) and in the middle of the Kondo ridge (right). These correspond to positions $A$ and $B$ in Fig.2, respectively. The difference between the superconducting state of the leads (solid line) and normal state (dashed line) is clearly observed. The peaks in the $dI/dV$ in the superconducting state are due to MAR.

$B = 26$ mT. The critical field of the electrodes was experimentally determined to be $\sim 12$ mT. Figure 2 shows a gray scale representation of the measured differential conductance $dI/dV_{sd}$ versus source-drain ($V_{sd}$) and gate voltage ($V_g$) at $T = 50$ mK with the leads in the normal state. Measured over a large range of $V_g$ we observe a series of truncated low-conduction Coulomb blockade diamonds linked by narrow ridges of high conductance of which Fig.2 is a small part, see also Ref.[6]. From these and other Coulomb diamonds at different $V_g$ we obtain an average charging energy $U_C = 0.45$ meV and an average level spacing $\delta\epsilon = 0.45$ meV, with $\delta\epsilon$ varying between 0.3 and 0.7 meV.

The high conductance ridge around $V_{sd} = 0$ mV in Fig.2 is a manifestation of the Kondo effect occurring when the number of electrons on the dot is odd and the total spin $S = 1/2$. At $T = 50$ mK the Kondo state seems to be fully developed and has reached the unitary limit with a conductance maximum of $2e^2/h$. The Kondo temperature $T_K$ can be estimated from the width of the Kondo ridge out of equilibrium [12]. The full width at half maximum (FWHM) corresponds to $\sim k_B T_K$ which yields a Kondo temperature for the ridge in Fig.2 of about 1.86 K. In total we have observed 12 Kondo ridges with Kondo temperatures varying between 0.52 and 3.34 K.

When the magnetic field is off, the leads are superconducting and the conductance pattern is dramatically different. This is illustrated by Fig.3 which compares $dI/dV$ in the normal (dashed lines) and superconducting state (solid lines) at the $V_g$ positions $A$ and $B$ of Fig.2. Whereas the $dI/dV$ in the normal state has no pronounced features (except for the Kondo resonance at position $B$), a series of peaks appear in the superconducting state. These are the signature of MAR. The peaks at $\pm 0.2$ mV correspond to the superconducting gap of $2\Delta$ and mark the onset of direct quasiparticle tunneling. The peaks at lower $V_{sd}$ involve one or more Andreev reflections. The observed subharmonic gap structure is discussed in more detail in Ref.[7]. The superconducting gap energy of $\Delta = 0.1$ meV is slightly less than the expected 0.18 meV for bulk aluminum which we attribute to the intermediate Au layer (necessary to obtain good electrical contact to the MWNT).

Whereas the conductance at $V_{sd} = 0$ mV in the superconducting state is less than its normal state value in the middle of an $S = 0$ Coulomb diamond, the situation is very different for the Kondo region. Here the conductance increases significantly and a resonance remains around $V_{sd} = 0$, albeit narrower than in the normal state. This has been observed for all Kondo resonances, provided $T_K \gtrsim \Delta$, see Ref.[6]. As stated in the introduction, here we focus on the low-bias region of those Kondo resonances in the superconducting state and try to identify signatures of Andreev states dynamics.

To describe theoretically a S-nanotube-S system we shall first assume that the level spacing $\delta\epsilon$ in the nanotube is large compared to the superconducting gap in the leads $\Delta$. In the actual case of the present experiments $\Delta \simeq 0.1$ meV and $\delta\epsilon \simeq 0.45$ meV, which means that this approximation is roughly correct. The problem can thus be mapped into a single-level Anderson model with a model Hamiltonian $H = H_L + H_R + H_T + H_D$, where $H_{L,R}$ describe the left and right leads as BCS superconductors, $H_T = \sum_{k,\sigma,\mu=L,R} t_\mu \hat{c}^\dagger_{k,\sigma} d_\sigma + \text{h.c}$, is the

term coupling the dot to the leads, $\hat{d}^\dagger_\sigma$ and $\hat{c}^\dagger_{k,\sigma}$ being creation operators for electrons in the dot and in the leads respectively. $H_D = \sum_\sigma \epsilon_0 \hat{n}_\sigma + U\hat{n}_\uparrow\hat{n}_\downarrow$ is the uncoupled dot Hamiltonian characterized by the dot level position $\epsilon_0$ and the Coulomb interaction $U$. It is assumed that the coupling of the dot to the leads in the normal state can be described by energy independent tunneling rates $\Gamma_{L,R}$.

A crucial point in the analysis of this model is how to deal with the electron correlation effects. In Ref. [13] a perturbative approach was used to study the zero-voltage case. It was found that the AS's in the Kondo regime ($T_K > \Delta$) have essentially the same phase dependence as in the non-interacting case but with a reduced amplitude. This is consistent with a Fermi liquid description of the normal state with renormalized parameters $\epsilon_0^*$ and $\Gamma^*_{L,R}$, where $\Gamma^*_L + \Gamma^*_R = 2\Gamma^* \simeq T_K$ fixes the width of the Kondo resonance. Although different approximations differ in the way to relate these quantities to the bare parameters, the description in terms of the renormalized ones can be considered as universal [14]. In the opposite limit ($T_K < \Delta$), the system is well described within the Hartree-Fock approximation [10, 13, 15].

This fully phase-coherent picture is limited in the actual system by the presence of inelastic scattering mechanisms not considered in the present model like electron-phonon interactions. We shall later discuss its effect in the quasiparticle current by introducing a phenomenological inelastic relaxation rate $\eta$.

In the zero-bias limit the Andreev states are determined by the poles of the dot retarded Green function which, in the approximation mentioned above can be written as

$$G^r_D(\omega) \simeq \frac{\Gamma^*}{\Gamma} \begin{pmatrix} \omega - \epsilon_0^* - 2\Gamma^* g^r & 2\Gamma^* f^r \cos\phi/2 + i\delta\Gamma^* \sin\phi/2 \\ 2\Gamma^* f^r \cos\phi/2 - i\delta\Gamma^* \sin\phi/2 & \omega + \epsilon_0^* - 2\Gamma^* g^r \end{pmatrix}^{-1}, \quad (1)$$

with $\delta\Gamma^* = \Gamma^*_L - \Gamma^*_R$, $g^r = -(\omega + i0^+)/\sqrt{\Delta^2 - (\omega + i0^+)^2}$ and $f^r = \Delta/\sqrt{\Delta^2 - (\omega + i0^+)^2}$ corresponding to the dimensionless Green functions of the uncoupled electrodes. In the electron-hole symmetric case ($\epsilon_0^* = 0$ and $\Gamma^*_L = \Gamma^*_R$) the AS's are then determined by the equation

$$\omega_s \pm \Delta \cos\phi/2 + \frac{\omega_s\sqrt{\Delta^2 - \omega_s^2}}{2\Gamma^*} = 0. \quad (2)$$

The solutions of Eq. (2) are plotted in Fig. 4. As can be observed the AS detach from the continuous spectrum and behave approximately as $\omega_s \sim \pm\widetilde{\Delta}\cos\phi/2$ with $\widetilde{\Delta} < \Delta$. The energy interval between the AS and the edges of the gap is given by $\Delta - \widetilde{\Delta} \simeq 2\Delta^3/(2\Gamma^*)^2$ for $\Gamma^* > \Delta$. On the other hand at the crossing between the two AS's ($\phi = \pm\pi$) $\widetilde{\Delta}$ can be approximated by $\Delta/(1 + \Delta/2\Gamma^*)$.

In a non-symmetric situation ($\epsilon_0^* \neq 0$ and/or $\Gamma^*_L \neq \Gamma^*_R$) the two ballistic states are coupled and there appear an upper and a lower bound state with an internal gap of the order of $2\Delta\sqrt{1-\tau}$, where $\tau = 4\Gamma^*_L\Gamma^*_R/\left[(\epsilon_0^*)^2 + (\Gamma^*)^2\right]$ is the normal transmission at the Fermi energy. This is similar to the behavior of the AS's in a point contact with finite reflection probability, except for the detachment from the continuous spectrum (see Fig. 4).

In the voltage biased case it can be assumed that the description in terms of the renormalized parameters $\epsilon_0^*$ and $\Gamma^*_{L,R}$ remains valid in the regime $eV \ll \Delta \sim T_K$ in which we are interested. Within the present model the current operator between the leads and the dot is given by

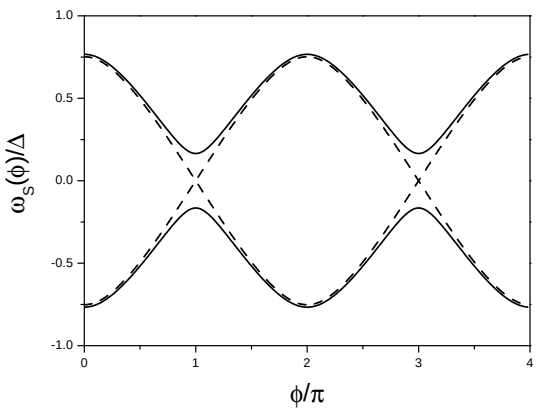


FIG. 4: Andreev states for a S-QD-S in the Kondo regime. Dashed and full lines correspond to a symmetric and non-symmetric situation respectively.

$$\hat{I}_\mu = \frac{ie}{\hbar}\sum_{k,\sigma}\left(t_\mu \hat{c}^\dagger_{k,\sigma} d_\sigma - \text{h.c}\right) \quad (3)$$

For calculating the average current we use the Keldysh formalism following previous works [16]. The main quantities to determined are the Keldysh Green functions in Nambu space given by $\hat{G}^{+-}_{ij}(t,t') = i < \hat{\psi}^\dagger_j(t')\hat{\psi}_i(t) >$, where $\hat{\psi}_i$ are the field operators in Nambu space defined as

$$\hat{\psi}_i = \begin{pmatrix} c_{i\uparrow} \\ c^\dagger_{i\downarrow} \end{pmatrix} \ , \ \hat{\psi}^\dagger_i = \begin{pmatrix} c^\dagger_{i\uparrow} & c_{i\downarrow} \end{pmatrix} \tag{4}$$

The average current can then be written as

$$I_\mu(t) = \frac{e}{\hbar}\mathrm{Tr}\left\{\hat{\sigma}_z\left[\hat{t}_\mu \hat{G}^{+-}_{D,\mu} - \hat{t}^\dagger_\mu \hat{G}^{+-}_{\mu,D}\right]\right\} \tag{5}$$

where $\hat{t}_\mu = t_\mu \hat{\sigma}_z$. One can integrate out the leads to find an expression of the current only in terms of the dot Keldysh Green function $\hat{G}^{+-}_D$, which is related to the retarded and advanced Green functions by

$$\hat{G}^{+-}_D = \hat{G}^r_D \hat{t}_L \hat{g}^{+-}_L \hat{t}^\dagger_L \hat{G}^a_D + \hat{G}^r_D \hat{t}_R \hat{g}^{+-}_R \hat{t}^\dagger_R \hat{G}^a_D \tag{6}$$

where $\hat{g}^{+-}_{L,R}$ are the Keldysh Green functions for the uncoupled electrodes, whose Fourier transform is given by $n_F^{L,R}(\omega)\left[\hat{g}^a(\omega) - \hat{g}^r(\omega)\right]$, $n_F^{L,R}(\omega)$ being the corresponding Fermi factor. In Eq. (6) integration over internal time arguments is implicitly assumed.

Using the different relations between Green functions in Keldsyh space the current between the dot and the left lead can be written as

$$I_\mu(t,V) = \frac{2e}{\hbar}\mathrm{ReTr}\left\{\hat{\sigma}_z\left[\hat{\Gamma}^r_\mu \hat{g}^{+-}_\mu + \hat{\Gamma}^{+-}_\mu \hat{g}^a_\mu\right]\right\} \tag{7}$$

where $\hat{\Gamma}_\mu = \hat{t}_\mu \hat{G}_D \hat{t}^\dagger_\mu$. In order to evaluate the current under fixed bias voltage a double Fourier transformation of the temporal arguments in the dot Green functions is performed, which leads to a set of algebraic equations for the different Fourier components [11, 16]. This procedure allows to evaluate the current as $I(t,V) = (I_L - I_R)/2 = \sum_n I_n(V) exp[in\phi(t)]$, where $\phi(t) = 2eVt/\hbar + \phi_0$. In the present case we shall be interested in the dc component $I_0(V)$.

The behavior of the dc current at low bias is shown in Fig. 5. When $\Gamma^* \gg \Delta$ the $IV$ characteristics of a ballistic quantum point contact is gradually recovered. As $\Gamma^*/\Delta$ is reduced the low bias conductance is gradually suppressed. When $\Gamma^* \sim \Delta$, MAR oscillations with a period $\Delta/n$, where $n$ is an integer, start to be observable in the $IV$ characteristic [8].

These results correspond to the fully phase-coherent case ($\eta = 0$) and, as can be observed, exhibit a highly non-linear behavior where a linear regime is strictly never reached. The presence of a finite $\eta$ in the actual system limits the observation of this behavior, giving rise to a linear regime in the limit $V \to 0$. This is illustrated in the right panel of Fig. 5 where the $IV$ characteristic for $\Gamma^* = 2\Delta$ is represented for different values of $\eta$. As can be observed, the current at low bias is extremely sensitive to the actual value of this parameter. Notice also that the oscillations with period $\Delta/n$ are suppressed for $eV \leq \eta$.

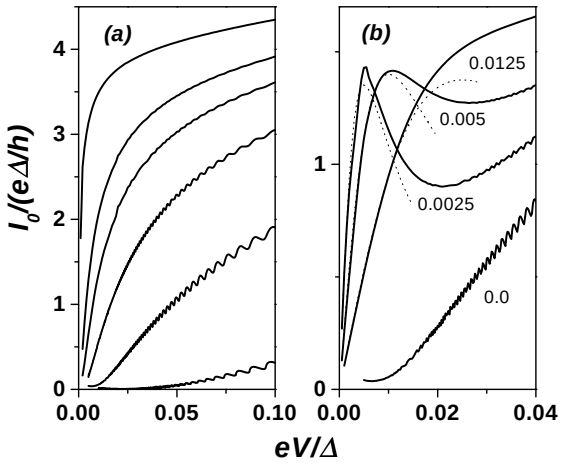


FIG. 5: Low bias current-voltage characteristic for the symmetric case. Panel (a) corresponds to the fully phase-coherent case ($\eta = 0$) and different values of $\Gamma^*/\Delta = 10$, 5, 4, 3, 2, 1 from top to bottom. Panel (b) corresponds to $\Gamma^*/\Delta = 2$ and different values of $\eta/\Delta$ as indicated. The dotted lines show the analytic description of the $eV < \eta$ regime given by Eq. (11).

These results can be understood more deeply by analyzing the dynamics of the Andreev states in the presence of an applied bias taking into account the finite relaxation rate. Let us first consider the symmetric case. In the limit $eV < \eta$ we can obtain the non-equilibrium occupation of the Andreev states, $\rho^\pm$, using the Boltzman equation in the relaxation time approximation, i.e.

$$\frac{\partial \rho^\pm}{\partial t} = -\frac{\rho^\pm - \rho^{(0)\pm}}{\tau} \tag{8}$$

where $\rho^{(0)\pm} = n_F\left[\pm\omega_S(\phi)\right]$ and $\tau = \hbar/2\eta$. In the stationary state these quantities can be expanded as $\rho = \sum_n \rho_n \exp in\omega_0 t$, where $\omega_0 = eV/\hbar$ and we obtain

$$\rho^\pm_n = \frac{\rho^{(0)\pm}_n}{1 + in\omega_0\tau} \tag{9}$$

At zero temperature the Fourier components of the equilibrium distribution are simply given by $\rho^{(0)\pm}_{2k+1} = (-1)^k/(\pi(2k+1))$. To calculate the current we first notice that within this approximation

$$I = \frac{e}{\hbar}\frac{\partial \omega_S}{\partial \phi}\left[\rho_+ - \rho_-\right] \tag{10}$$

Averaging this expression to obtain the dc current, assuming that $\omega_S \simeq \widetilde{\Delta}\cos\phi/2$, yields

$$I_0 = \frac{2e^2\widetilde{\Delta}}{h\eta}\frac{V}{1+(eV/2\eta)^2} \qquad (11)$$

This expression indicates that the conductance reaches a maximum at $V = 0$ where it takes the value $G(0) = 2e^2\widetilde{\Delta}/(h\eta)$ and decreases with $V$ defining a zero-bias conductance peak with a typical width fixed by $\sim \eta$. In panel (b) of Fig. 5 we compare the results of this approximation with the full numerical ones. As can be observed Eq. (11) describes correctly the behavior for $eV < \eta$.

This description can be straightforwardly generalized to a non-symmetric situation. In this case the effect of the transition between the lower and the upper state can be analyzed as a Landau-Zener process with probability $p = \exp(-\pi r\Delta/eV)$, where $r = 1-\tau$ [17]. The current in Eq. (11) will be then suppressed by a factor $p$.

On the other hand for finite temperature $T$, we obtain $I_0(T) = I_0(T=0)F(T)$, where $I_0(T=0)$ is given by Eq. (11) and

$$F(T) = \frac{2\pi}{\beta\widetilde{\Delta}}\sum_{m=0}^{\infty}\left(1-\frac{x_m}{\sqrt{1+x_m^2}}\right) \qquad (12)$$

where $\beta = 1/k_BT$ and $x_m = (2m+1)\pi/(\beta\widetilde{\Delta})$. The absence of any dependence on $\eta$ or $V$ in $F(T)$ indicates that the main effect of temperature is to introduce a global scale factor reducing the magnitude of the conductance.

This simple theory can be used to analyze the low bias conductance peak in the experimental results. As shown in Fig. 6, this peak can be well fitted by the expression (11) using $\eta$ and $\widetilde{\Delta}$ as free parameters. The values of $\eta$ thus obtained are rather constant (between $\sim 10$ and $\sim 15\mu eV$) while $\widetilde{\Delta}$ strongly depends on $T_K$. This behavior is consistent with our theoretical model in which the inelastic relaxation rate is a fixed parameter set by some microscopic mechanism not explicitly included in the model. Notice that $\eta$ is considerable smaller than both $\Delta$ and $\delta\epsilon$. On the other hand the theory predicts an increase of $\widetilde{\Delta}$ as a function of $T_K$ roughly given by $\widetilde{\Delta}/\Delta \simeq 1/(1+\Delta/T_K)$. In the lower right pannel of Fig. 6 this prediction is compared with the fitted experimental values. Notice that, in spite of the rather large dispersion in the data, both the order of magnitude and the general trend are in agreement with the theoretical predictions.

In conclusion we have presented a combined theoretical and experimental analysis of electron transport in carbon nanotubes coupled to superconducting leads. The differential conductance in the Kondo regime exhibits a zero bias peak which can be related to the dynamics of the subgap Andreev states under an applied bias voltage. A main ingredient that has to be included in the model in order to account for the experimental results is a finite relaxation rate $\eta$ which gives rise to a linear regime in the low bias limit $eV < \eta$. The different mechanisms that can contribute to this finite rate can be either intrinsic (like electron-phonon coupling within the nanotube) or extrinsic (for instance due to phase diffusion like in a RSJ model [9]). Further experiments could be of interest in order to elucidate this issue.

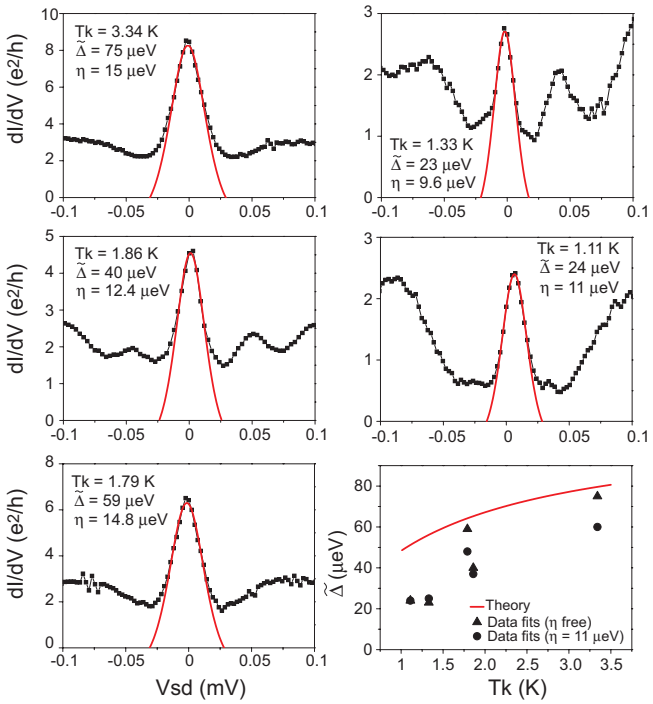


FIG. 6: Differential conductance in the middle of 5 different Kondo ridges with decreasing $T_K$. The red lines are fits to the data using Eq.11. The lower right pannel shows the fitted values of $\widetilde{\Delta}$ vs $T_K$ compared to the theoretical prediction $\widetilde{\Delta}/\Delta \simeq 1/(1+\Delta/T_K)$.

The authors would like to thank J.C. Cuevas for useful discussions. Work was supported by EU through DIENOW Research Training Network.

* Present address: Cavendish Laboratory, Cambridge, UK.

[1] W. Liang et al., Nature **411**, 665 (2001).
[2] A. Bachtold et al., Nature **397**, 673 (1999).
[3] M. Bockrath et al., Nature **397**, 598 (1999).
[4] J. Nygård, D.H. Cobden and P.E. Lindelof, Nature **408**, 342 (2000); M.R. Buitelaar et al., Phys. Rev. Lett. **88**, 156801 (2002).
[5] A. Kasumov et al., Science **284**, 1508 (1999).
[6] M.R. Buitelaar et al., Phys. Rev. Lett. **89**, 256801 (2002).
[7] M. R. Buitelaar et al., Phys. Rev. Lett. **91**, 057005 (2003).
[8] A.L. Yeyati, A. Martín-Rodero and E. Vecino, Phys. Rev. Lett. **91**, 266802 (2003).
[9] Choi et. al., cond-mat/0312271.

[10] Y. Avishai et al., Phys. Rev. B **63**, 134515 (2001); Phys. Rev. B **67**, 041301 (2003).
[11] A.L. Yeyati et al., Phys. Rev. B **55**, R6137 (1997); G. Johansson et al., Physica C **293**, 77 (1997).
[12] Y. Meir, N.S. Wingreen, and P.L. Lee, Phys. Rev. Lett. **70**, 2601 (1993); D. Goldhaber-Gordon et al., Phys. Rev. Lett. **81**, 5225 (1998).
[13] E. Vecino et al., Phys. Rev. B **68**, 035105 (2003).
[14] An equivalent description in terms of renormalized parameters is obtained within the slave-boson mean field approach. See for instance last reference in [10].
[15] A.V. Rozhkov and D.P. Arovas, Phys. Rev. Lett. **82**, 2788 (1999); Phys. Rev B **62**, 6687 (2000). A.A. Clerk and V. Ambegaokar, Phys. Rev. B **61**, 9109 (2000).
[16] J.C. Cuevas et al., Phys. Rev. B **54**, 7366 (1996); A. Martín-Rodero et al., Superlattices Microstruct. **25**, 927 (1999).
[17] D. Averin and A. Bardas, Phys. Rev. Lett. **75**, 1831 (1995).